Microkinetic Modeling of the CO + NO Reaction on Pd/MgO Particles

Geoffroy Prévot* and Claude R. Henry

CRMC2,† CNRS, Campus de Luminy, Case 913, 13288 Marseille Cedex 09, France

Received: March 11, 2002; In Final Form: August 19, 2002

Several experimental studies have shown the ability of Pd for the NO + CO conversion. In particular, a coherent set of results have been obtained on Pd particles supported on MgO, both concerning steady state conditions and transient regimes, temperature, and pressure dependence of the reaction rate. In this paper, we describe a microkinetic modeling of this reaction by numerical integration of the differential equations governing the different concentrations. The model is taken as simple as possible with only one type of reactive site. Parts of the parameters have been taken in order to fit specific experimental results. The simulation results agree qualitatively very well with the whole set of experiments. They clearly demonstrate that the rate-limiting step is, at low temperature, the NO decomposition and, at high temperature, the CO adsorption. The differences between experiments and simulations, beyond the intrinsic heterogeneity of the experimental set of results, reflect the approximations of the model. Nevertheless, the temperature and pressure dependence of the CO_2 production rate are correctly reproduced by the simulations as well as major features of the transient signals.

I. Introduction

The CO + NO reaction is a key reaction for air pollution control. Whereas industrial catalytic converters contain mainly Pt and Rh particles, the use of Pd, which is more abundant, could reduce the fabrication cost of the catalyst. The CO + NO reaction on Pt catalysts has attracted considerable interest since the discovery of kinetic oscillations in the low-pressure range.[1,2] This reaction has also been intensively studied for Rh catalysts, which easily dissociate the NO molecule (for a review, see ref 3), but much less studies have been devoted to the CO + NO reaction on Pd catalysts, and to our knowledge, no kinetic modeling of the reaction on Pd has been proposed. The different Pd catalysts studied range from single crystals, for example, Pd(111),[4] Pd(100),[4,5] Pd(110),[6] and Pd (320),[7] to supported Pd particles, for example, Pd/SiO_2,[8] Pd/Al_2O_3,[9] or Pd/MgO.[10,11] Goodman and co-workers have compared the activity of different Pd catalysts under high-pressure conditions (a few Torr).[12] The single crystals, especially Pd(111), are found to be more reactive than supported particles. This has been explained by a poisoning of the reactive site of the particles by adsorbed N atoms. The small particles present a high number of low-coordinated atoms. The chemisorption is stronger on these adsorption sites: N atoms do not desorb and hinder further NO decomposition. The limiting processes under low-pressure conditions could be very different. For Pd/MgO,[11] it has been shown that the NO decomposition was the rate-limiting step (RLS) at low temperature, whereas at high temperature, the CO adsorption was the RLS, because of fast CO desorption. Recent ab initio calculations for flat and stepped Pd(100) and Pd(111) surfaces[13] confirm these assumptions: for every adsorption site considered, the higher barrier calculated is the energy barrier for NO dissociation and the barrier for CO desorption is higher than for CO oxidation, which favors desorption at high temperatures. To compare the energy barriers to the experiments, kinetic modeling of the reaction is needed.

In this paper, we describe the kinetic modeling of the CO + NO reaction on Pd/MgO particles, under low-pressure conditions. Different experimental studies have been performed on this system by molecular beam relaxation spectroscopy (MBRS). The CO[14−16] and NO[17] adsorption, the CO oxidation,[18−20] and the CO + NO reaction[10,11,21,22] have been studied as a function of substrate temperature, NO or CO pressure, and size and morphology of the particles. In the experimental setup, one of the gases is introduced as a molecular beam at a fixed flux whereas a leak valve controls the isotropic pressure of the other gas. The desorption products are measured with a mass spectrometer.

An analytical model has been developed by Piccolo et al.[20] for describing the reaction between CO and a preadsorbed oxygen layer. As the initial surface considered was fully saturated with oxygen, care was taken to the concentration dependence of the CO sticking coefficient. The simulation results are in good agreement with the main experimental features observed; in particular, the decrease of this sticking coefficient with oxygen concentration allows us to explain the delay in the CO_2 production rate. In the following, we propose a similar analysis of the CO + NO reaction to describe the experimental results[10,11,21,22] obtained.

II. Reaction Mechanism

Following the work of Piccolo et al.,[10,11] we have considered the following mechanism for the reaction:

$$NO_g \leftrightarrow NO_a \quad (1)$$

$$NO_a \rightarrow N_a + O_a \quad (2)$$

$$CO_g \leftrightarrow CO_a \quad (3)$$

* To whom correspondence should be addressed. GPS, UMR CNRS 7588, Universités Paris 6 et 7, Tour 23, 2, Place Jussieu, 75251 Paris Cedex 05, France. Tel: 33-1-44-27-46-53. Fax: 33-1-43-54-28-78. E-mail: prevot@gps.jussieu.fr.

† CRMC2 is associated with the Universities of Aix Marseille II and III.

10.1021/jp0257451 CCC: $22.00
Published on Web 11/06/2002

$$CO_a + O_a \rightarrow CO_{2g} \quad (4)$$

$$N_a + N_a \rightarrow N_{2g} \quad (5)$$

$$O_a \rightarrow O_{bulk} \quad (6)$$

where the symbols a and g indicate, respectively, the chemisorbed and the gas phase.

This mechanism is practically the same as the one proposed by Belton for the CO + NO reaction on Rh(111).[23] As was done by Zhdanov and Kasemo[3] in their numerical simulations of this reaction on Rh, we do not take the N_2O formation into account. Whereas an important N_2O peak is observed by temperature programmed reaction on Pd single crystals after adsorption of NO,[24] this production has been always found negligible on Pd/MgO particles, either for pure NO adsorption or during reaction with CO.[10,11]

Let us briefly discuss the other hypotheses. The mechanism is of the Langmuir−Hinshelwood type, i.e., the reaction takes place after adsorption of both molecules. Only NO dissociates; the CO dissociation is very unlikely.[15] We do not consider any CO_2 adsorbed at the surface since the desorption of CO_2 is very fast. For simplicity, we made the same assumption for the nitrogen molecules. In fact, the limitation of N_{2g} production by either N_{2a} formation or N_{2a} desorption does not significantly modify the simulation results. The last equation has been added in order to take account for the O_a vanishing observed on the Pd particles.[22] As no O_2 desorption signal is observed at the temperatures studied ($T < 400$ °C),[17] the oxygen must diffuse toward the bulk. This diffusion of oxygen in the subsurface region has already been observed on Pd both for particles[25,26] and for single crystals.[27,28] In the case of small particles, the total amount of oxygen that can be adsorbed in the bulk is limited by the size of the particles. Nethertheless, experiments[17] of NO adsorption and decomposition on Pd particles indicate that the total amount of oxygen adsorbed in the bulk could not exceed 1 monolayer (ML) for 1 h adsorption under 5×10^{-8} Torr of NO. For 10 nm particles, it corresponds to a mean oxygen concentration of 0.1 oxygen per Pd atom. In the time scale of the experiments and simulations, the total amount of oxygen in the particles remains then always small.

III. Numerical Procedure

The simulations are based on the numerical integration of the kinetic equations. In this mean field approach, one considers mean values for the different concentrations: [CO], [NO], [N], and [O]. These values are the same for each particle and do not depend on the type of site considered on the Pd cluster ((100) or (111) facet, corner or edge site...). This is a crude approximation as already pointed out in recent review papers.[29,30] On low-coordinated atoms (corner and edge sites), the activation barriers for the elementary reactions are generally smaller,[31] but the molecules are also more strongly bound. These sites can thus be rapidly poisoned by strong chemisorbed atoms or molecules and become inactive. For medium size Pd particles (10 nm), the step edge and corner atoms represent less than 10% of the total Pd surface atoms. It seems therefore reasonable to only consider facet sites. Moreover, we do not make any difference between (111) terraces and (100) terraces; in fact, before the regime of coalescence, the proportion of (111) facet sites is much higher than the proportion of (100) facet sites.[29] To summarize, the reaction kinetics depends only on the mean concentrations. The time evolution of these concentrations is thus simply derived from the reaction mechanism considered above:

$$d[CO]/dt = \alpha_{gCO} F_{CO} s_{CO} - \nu_{oxy}[CO][O] - \nu_{dCO}[CO]$$

$$d[NO]/dt = \alpha_{gNO} F_{NO} s_{NO} - \nu_{dec}[NO] - \nu_{dNO}[NO]$$

$$d[O]/dt = \nu_{dec}[NO] - \nu_{oxy}[CO][O] - \nu_{diff}[O]$$

$$d[N]/dt = \nu_{dec}[NO] - 2\nu_{for}[N][N]$$

$\alpha_{gCO}F_{CO}$ (respectively, $\alpha_{gNO}F_{NO}$) is the total CO (respectively, NO) flux incoming on a Pd particle. It represents either a molecular beam flux or an isotropic pressure. In both cases, there are two contributions to the flux: direct flux of molecules on the cluster, F_{CO} (respectively, F_{NO}), and indirect flux through the oxide support. In this reverse spillover mechanism, observed for both CO[16,32] and NO,[17] some of the molecules physisorbed on the oxide substrate diffuse toward the Pd clusters where they become chemisorbed. This indirect contribution is temperature-dependent: it is more important at low temperature for which the diffusion length of the molecules on MgO is higher (desorption-limited diffusion). It also depends on the characteristics of the catalyst; this effect is more pronounced for particles covering a low fraction of the surface. We have used in the simulations the measured experimental values,[16,17] fitted by simple analytical laws. In the high temperature regime, the only contribution comes from the direct flux and $\alpha_{gCO} = 1$ (respectively, $\alpha_{gNO} = 1$). In the low-temperature regime, all of the CO (respectively, NO) molecules, which are physisorbed on the MgO substrate, diffuse toward the Pd particles and $\alpha_{gCO} = 1 + (1 - Ac)/Ac \times \alpha_{CO/MgO}$ (respectively, $\alpha_{gNO} = 1 + (1 - Ac)/Ac \times \alpha_{NO/MgO}$). $\alpha_{CO/MgO} = 0.5$ (respectively, $\alpha_{NO/MgO} = 0.6$) is the adsorption probability of CO (respectively, NO) on MgO, experimentally determined,[16,17] and Ac is the fraction of the MgO surface covered by the particles. The transition temperature between these two regimes is approximately 250 °C. We have simulated medium size (10 nm) Pd clusters, for which the effective catalytic activity is the highest.[10] As they cover 33% of the MgO surface, the low-temperature value of α_{gCO} (respectively, α_{gNO}) is 2 (respectively, 2.2).

s_{CO} (respectively, s_{NO}) is the CO (respectively, NO) sticking coefficient. These sticking coefficients are a priori concentration and temperature-dependent. For example, for CO adsorption on Pd, a precursor state associated to physisorbed CO has been evidenced on polycrystalline Pd.[33] The competition between desorption and chemisorption from this precursor state results in a complex temperature dependence of the sticking coefficient. In our case, four different chemisorbed species are present at the Pd surface. It is impossible to obtain, from an experimental study, sufficient information on the concentration dependence of the sticking coefficients. To simplify our calculations, we have chosen very simple laws for the sticking coefficients:

$$s_{CO} = s^0_{CO} \text{ for } [CO] < [CO]_{sat}$$

and

$$s_{NO} = s^0_{NO}\,(1 - ([N] + [NO])/[N_t]_{sat})$$

We use the value of the saturation coverage $[CO]_{sat} = 0.5$ measured on Pd(111).[34] $[N_t]_{sat}$, which is the total N + NO saturation coverage, is also taken to 0.5. The initial sticking coefficients s^0_{CO} and s^0_{NO} are close to unity.[35,36] In our simulations, they are taken equal to unity.

The different frequencies ν_{dCO}, ν_{dNO}, ν_{dec}, ν_{oxy}, ν_{for}, and ν_{diff}, corresponding, respectively, to desorption of CO, desorption of

NO, decomposition of NO, oxidation of CO, N_2 formation, and diffusion of oxygen into the bulk, are temperature-dependent:

$$\nu_{dCO} = \nu^0_{dCO} \exp(-E_{dCO}/kT)$$

$$\nu_{dNO} = \nu^0_{dNO} \exp(-E_{dNO}/kT)$$

$$\nu_{dec} = (1 - x_{tot}) \times \nu^0_{dec} \exp(-E_{dec}/kT)$$

$$\nu_{for} = \nu^0_{for} \exp(-E_{for}/kT)$$

$$\nu_{oxy} = \nu^0_{oxy} \exp(-E_{oxy}/kT)$$

$$\nu_{diff} = \nu^0_{diff} \exp(-E_{diff}/kT)$$

The activation energies are a priori concentration-dependent.[37] Experiments[14] have shown that for CO, the activation energy for the desorption E_{dCO} is constant for moderate coverage whereas E_{dNO} strongly decreases with NO coverage. We have taken a constant value for E_{dCO}: $E^0_{dCO} = 27$ kcal/mol with an attempt frequency of 5×10^{11} Hz. This value has been experimentally measured on the Pd particles before each experiment of the CO + NO reaction.[22] For the desorption of NO, the activation energy decreases with total coverage θ_{tot} above a critical concentration θ_0. This can be described with an analytical form with no discontinuities of the derivatives: $E_{dNO} = E^0_{dNO} - \gamma A_{dNO} \times \ln(1 + \exp(-\theta_0/\gamma) \times (\exp(\theta_{tot}/\gamma) - 1))$. The fit to the experimental values[21] leads to $E^0_{dNO} = 34$ kcal/mol, $A_{dNO} = 44$ kcal/mol, $\theta_0 = 0.14$, and $\gamma = 0.02$, for an attempt frequency of 1.3×10^{13} Hz. The activation energy for NO decomposition is also coverage-dependent:[17] $E_{dec} = E^0_{dec} - A_{dec}\theta_0$ with $E^0_{dec} = 30$ kcal/mol and $A_{dec} = 40$ kcal/mol, for an attempt frequency of 6.2×10^{10} Hz. These values have been adjusted on the experimental values[22] of the CO_2 production rate at $T = 250$ °C for different NO pressures (see Figure 1).

The other activation energies are taken constant; the activation energy for N_2 formation was taken arbitrarily low: $E_{for} = 20$ kcal/mol and $\nu^0_{for} = 5 \times 10^{12}$ Hz, to reproduce the abrupt decay of the N_2 desorbing flux when closing the NO beam.[21] As already mentioned, we do not take into account the presence of strongly bound nitrogen for which the N_2 formation energy should be much higher. The value for bulk diffusing oxygen was directly obtained from the experiments:[22] $E_{diff} = 2.35$ kcal/mol and $\nu^0_{diff} = 0.05$ Hz. E_{diff}, which is derived from the Arrhenius dependence of ν_{diff}, is very small and cannot be considered as the activation energy of an elementary process. The diffusion of oxygen in the bulk is certainly a complex mechanism with several elementary steps, and the choice of an Arrhenius dependence of ν_{diff} is done only for simplicity. Finally, we take for the CO oxidation $E_{oxy} = 21$ kcal/mol and $\nu^0_{oxy} = 5 \times 10^{10}$ Hz. To summarize, the activation energies of only two processes are concentration-dependent; they concern the desorption and the decomposition of NO. Of course, it is possible to include concentration effects for the other processes; for example, the desorption energy of CO and the activation energy for CO oxidation should be reduced at high coverage. Nevertheless, it is not necessary to take these effects into account in order to explain the major part of the experimental results. We have thus chosen to keep a relatively simple set of parameters. This whole set of parameters is indicated in Table 1.

The integration of the kinetic equations is done with a time step depending on the temperature. This integration gives the transient signals and, in the long times limit, the steady state reaction rate.

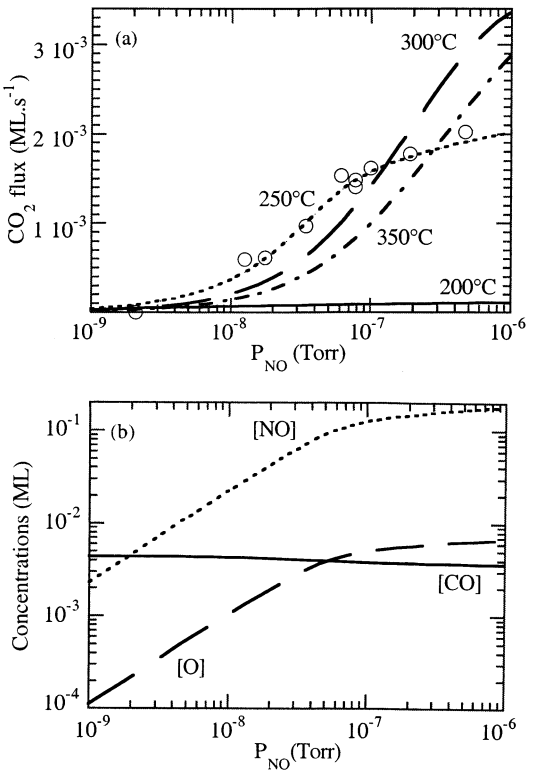

Figure 1. (a) Steady state CO_2 production rate as a function of the NO pressure, for a CO beam flux equivalent to 5×10^{-8} Torr and for different temperatures; the experimental measurements at 250 °C (dots) are taken from ref 22. (b) Steady state CO, NO, and O coverages as a function of the NO pressure, at constant CO beam flux, equivalent to 5×10^{-8} Torr and at $T = 250$ °C.

TABLE 1: Parameters Used for the Different Temperature-Activated Processes of the CO + NO Reaction[a]

process	E_0 (kcal/mol)	ν_0 (Hz)	A (kcal/mol)	θ_0	γ
NO desorption	34	1.3×10^{13}	44	0.14	0.02
NO decomposition	30	6.2×10^{10}	40		
CO desorption	27	5×10^{11}			
CO oxidation	21	5×10^{10}			
N_2 formation	20	5×10^{12}			
O diffusion in the bulk	2.35	0.05			

[a] Parameters A, θ_0, and γ refer to the coverage dependence of the activation energy (see text).

Two types of experiments are simulated. The first ones, hereafter mentioned as "CO beam" experiments[22] correspond to reaction under isotropic and variable NO pressure; the CO flux can be modulated in time to either a constant value $F_{COinc} = 1.9 \times 10^{13}$ mol cm^{-2} s^{-1} or a null value. The second ones mentioned as "NO beam" experiments[10,11] correspond to the reverse situation with a NO flux of $F_{NOinc} = 2.0\ 10^{13}$ mol cm^{-2} s^{-1}. Such molecular beam flux corresponds to an equivalent isotropic pressure of 5×10^{-8} Torr. Different quantities are calculated, the adsorbate concentrations [CO], [NO], [N], and [O] and the desorption fluxes f_{CO}, f_{NO}, f_{N_2}, and f_{CO_2}. The turnover number of the reaction (TON) is the number of CO_2 molecules produced per time unit and per Pd surface atom, i.e., the CO_2 flux normalized to the number of active sites.

For CO beam calculations, we define the reaction probability under steady state condition by the ratio $\eta = f_{CO_2}/f_{COinc}$, whereas for NO beam calculations, the reaction probability under steady state condition is defined by the ratio $\eta = f_{CO_2}/f_{NOinc}$.

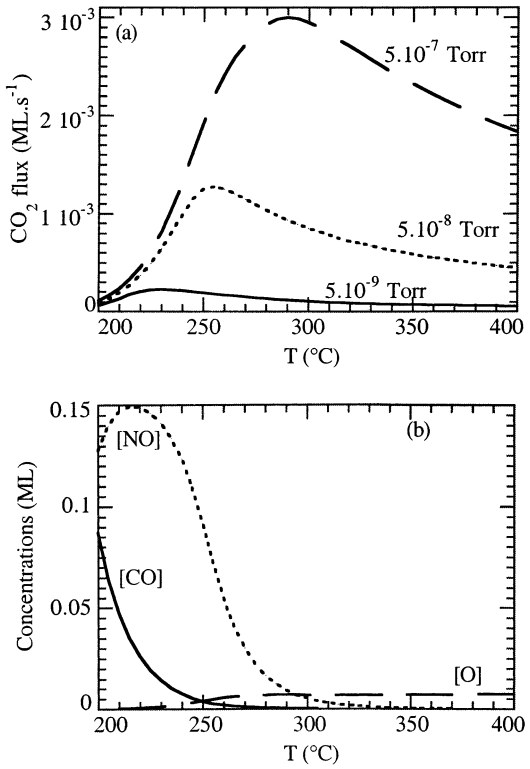

Figure 2. (a) Steady state CO_2 production rate as a function of the temperature, for a CO beam flux equivalent to 5×10^{-8} Torr, and various NO pressures. (b) Steady state CO, NO, and O coverages as a function of the temperature, at a NO pressure of 5×10^{-8} Torr, and at a constant CO beam flux, equivalent to 5×10^{-8} Torr.

IV. Results and Discussion

A. CO Beam Steady State TON. In this first series of simulations, the CO flux is kept constant and the NO pressure is variable. On Figure 1a is displayed the steady state reaction rate as a function of NO pressure for different temperatures. The TON increases nonlinearly with NO pressure; above a critical pressure, the slope is lowered. For $T = 250$ °C, this corresponds to a NO pressure of the order of 10^{-7} Torr. This variation is due to the fact that NO desorption is easier at high coverage whereas NO decomposition is lower. Both phenomena are needed in order to adjust the experimental results to the simulation ones. The values of the variation with concentration of the activation energy for NO decomposition have been obtained by fitting the experimental results at $T = 250$ °C. For the pressure range studied, no saturation of the TON with increasing NO pressure can be observed, even at 200 °C. In fact, at high pressure, only a small proportion of NO molecules react but this is compensated by the fact that the NO concentration is high. The steady state concentrations calculated at 250 °C are represented on Figure 1b. The NO and O concentrations are practically proportional. Above 10^{-7} Torr, the O and NO concentrations saturate due to the coverage dependence of the activation energies for NO desorption and decomposition.

The steady state CO_2 production rate as a function of temperature for various NO pressures is represented on Figure 2a. The evolution of the CO, NO, and O coverages with temperature for $P_{NO} = 5 \times 10^{-8}$ Torr is given on Figure 2b. The reaction rate increases rapidly to a maximum value, at a temperature T_{max}, and decreases slowly with temperature. The value of T_{max} increases from 230 to 290 °C when increasing the NO pressure from 5×10^{-9} to 5×10^{-7} Torr. This is an effect of the concentrations variation: at lower temperature, the partial CO and NO coverage and the total coverage are higher (see Figure 2b). The NO decomposition is lowered, which limits the reaction. The more important the NO pressure is, the higher T_{max} is. The decrease of the NO coverage at very low temperature ($T < 220$ °C) that can be seen on Figure 2b is due to the increase of the CO concentration, which consequently reduces the desorption energy of NO. However, in this high concentration regime, our simplified model cannot take into account the concentration dependence of all processes: the desorption energy of CO is also certainly reduced at this high coverage. Taking this dependence into account would lead to a different temperature dependence of the CO and NO concentration in the low temperature regime but would not drastically affect the global behavior of the TON.

In the high-temperature regime, the CO_2 production is determined by the competition between the different mechanisms. For an adsorbed NO molecule, the competition between desorption and decomposition affects the oxygen concentration. As for NO, in the limit of low concentrations, the desorption energy is higher than the activation energy for decomposition, the proportion of NO molecules that decompose decreases with temperature. For an adsorbed CO molecule, the competition between desorption and oxidation determines the CO_2 production rate. As the activation energy for oxidation is lower than the desorption energy, the proportion of CO molecules that react with oxygen decreases with temperature. It is worth noting that the oxygen concentration is practically constant at high temperatures.

B. NO Beam Steady State TON. In this second series of simulations, the NO flux is kept constant and the CO pressure is variable. The variation of the CO_2 steady state production rate with CO pressure for four different temperatures is given in Figure 3a. Each curve has a similar behavior: the TON first increases with CO pressure, then reaches a maximum at P_{COmax}, and finally decreases for high CO pressures. The TON at P_{COmax} depends on the temperature. The maximum production rate is obtained for the curve at $T = 250$ °C. The value of P_{COmax} also depends on the temperature; it is higher for high temperatures. This result fully agrees with the experimental observations of Piccolo et al. (Figure 3c from ref 10). The relative positions of the different curves corresponding to various temperatures are well-reproduced. Nevertheless, there is a scale factor between the experimental and the simulation results. This can be due to the fact that these experiments were performed on smaller particles (2.8 nm instead of 10 nm). The catalytic activity of such particles differs from the one of bigger particles. Moreover, these particles cover a small fraction of the MgO surface (only 11%). In that case, spillover effects are important and the total incident flux on the particles is much higher than in the case of the 10 nm particles studied for the simulations.

Nevertheless, one has also to consider the fact that the two experimental conditions are different. First of all, some uncertainties are related to the experimental calibration of the CO and NO beam. Second, in the case of NO beam experiments, when the beam is closed, there is only CO adsorption and desorption due to the isotropic CO pressure introduced in the chamber. In the case of CO beam experiment, NO molecules permanently dissociate at the surface. The total exposure to NO is much higher than in the case of the NO beam, and nitrogen or oxygen atoms can slowly poison the catalyst. It has been shown[17] that after the first NO adsorption−desorption cycles, the activity of the Pd particles was strongly reduced; this was attributed to strongly bound nitrogen atoms or to subsurface oxygen. In the simulation, there is only one type of nitrogen

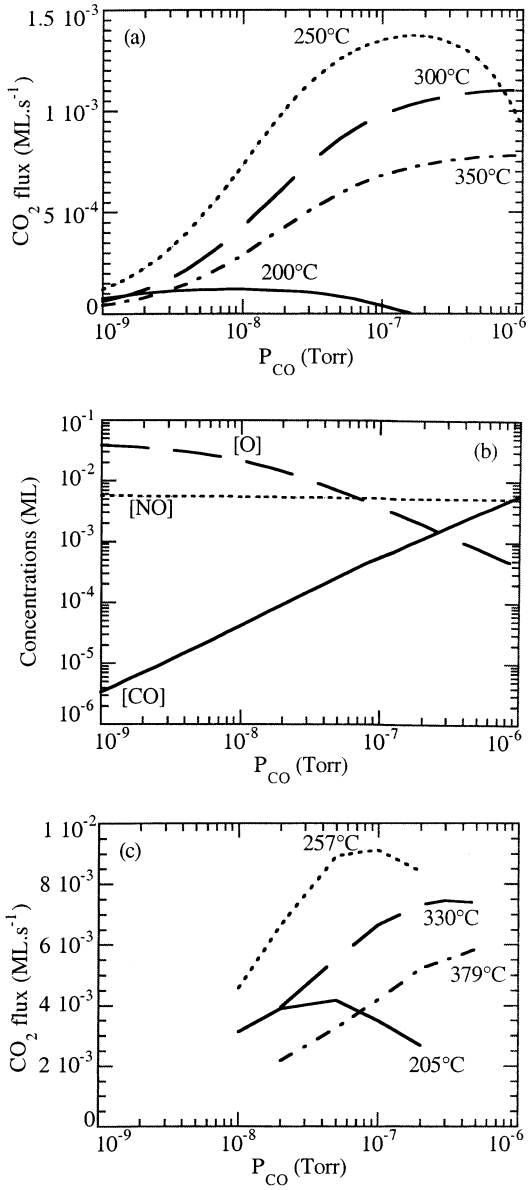

Figure 3. (a) Steady state CO_2 production rate as a function of the CO pressure, for a NO beam flux equivalent to 5×10^{-8} Torr. (b) Steady state CO, NO, and O coverages as a function of the CO pressure, for a NO beam flux equivalent to 5×10^{-8} Torr and at $T = 250$ °C. (c) Experimental steady state CO_2 production rate as a function of the CO pressure, obtained on 2.8 nm Pd/MgO particles, for a NO beam flux equivalent to 5×10^{-8} Torr (from ref 10).

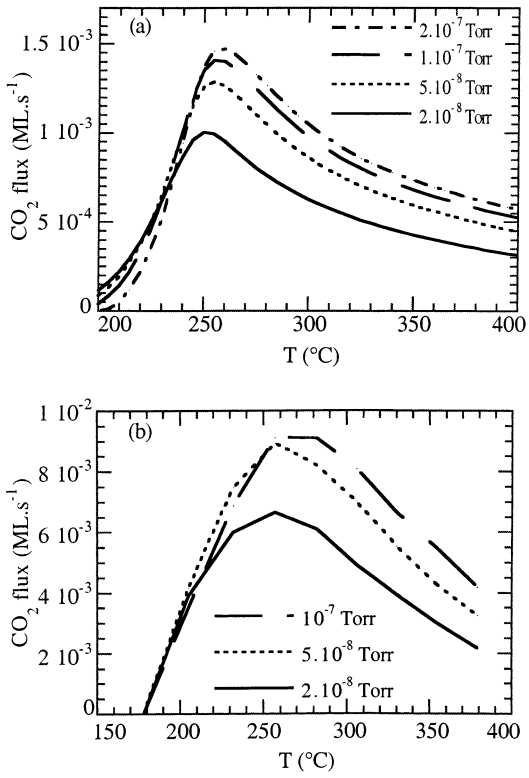

Figure 4. (a) Steady state CO_2 production rate as a function of the temperature, for a NO beam flux equivalent to 5×10^{-8} Torr, and various CO pressures. (b) Experimental CO_2 production rate as a function of the temperature, obtained on 2.8 nm Pd/MgO particles, for a NO beam flux equivalent to 5×10^{-8} Torr, and various CO pressures (from ref 11).

atom, which is weakly bound, and the reduction of the catalytic activity by subsurface oxygen is not taken into account. This can thus explain the difference between the two types of experiments.

The variation of the CO, NO, and O coverages with NO pressure is indicated in Figure 3b. The CO coverage increases of course with CO pressure, while the oxygen coverage decreases with CO pressure, due to the consumption of atomic oxygen by adsorbed CO molecules. The NO concentration is quasiconstant. The previous explanations also hold for these various behaviors. Increasing the CO pressure leads to higher CO coverages and thus to a higher CO_2 production rate. Nevertheless, if the CO coverage is too high, the decomposition of NO is hindered and the TON decreases. This effect is less pronounced at high temperature, and thus, P_{COmax} increases with T. The temperature dependence of the TON is of course similar to the one calculated in CO beam conditions. It is represented in Figure 4a for different CO pressures. The calculated and experimental (Figure 4b, from ref 11) curves show a similar behavior. At high temperature, the maximum TON is obtained for the higher CO pressure, whereas at low temperature, the minimum TON is obtained for the higher CO pressure, but the different curves are very close together. This proves clearly that the RLS at high temperature is the CO adsorption. Nevertheless, some differences can be seen; the experimental values are higher than the simulated ones, as already mentioned in the case of Figure 3. The shapes of the experimental and simulated curves are also slightly different; the simulated curves are narrower than the experimental ones. These differences reflect the very crude choice for coverage dependence of the activation energy for NO desorption and decomposition.

We have also studied the NO adsorption and decomposition when no CO is present. The evolution of the N_2 production rate with temperature is represented on Figure 5, together with the signal obtained with a CO pressure of 5×10^{-8} Torr (for such conditions, the N_2 signal is almost equal to half the CO_2 signal). The N_2 production rate is lower when no CO is present; in that case, the oxygen coverage is very high and hinders further decomposition of NO molecules. Oxygen atoms are not consumed by CO molecules but only diffuse in the bulk of the particles. This reduction of the N_2 production in the absence of CO is particularly pronounced in the intermediate temperature domain. At zero CO pressure, there is no straight maximum of the N_2 production; after a rapid increase in the 200−250 °C temperature domain, the N_2 production rate is practically constant. This is due to the fact that the activation energy for NO decomposition is close to the NO desorption energy. The N_2 flux is proportional to the probability for a NO molecule to decompose. In the high-temperature limit, it is given by the ratio

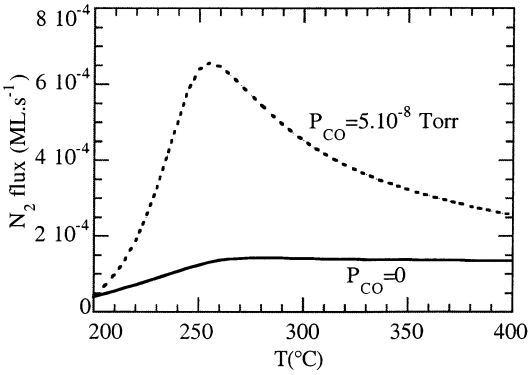

Figure 5. Steady state N_2 production rate as a function of the temperature, for a NO beam flux equivalent to 5×10^{-8} Torr, either without CO or with a CO pressure of 5×10^{-8} Torr.

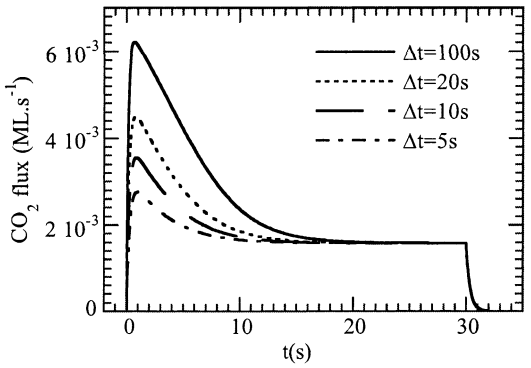

Figure 6. Transient CO_2 production rate at 250 °C. The CO beam flux is equivalent to 5×10^{-8} Torr and $P_{NO} = 10^{-7}$ Torr. The CO beam is open at $t = 0$ s and closed at $t = 30$ s. The time indicated for each curve corresponds to the waiting time between the previous CO beam closing at $t = -\Delta t$ and the CO beam opening at $t = 0$ s.

$(1 - x_{tot}) \times \nu^0_{dec}/\nu^0_{dNO}$, with $x_{tot} \approx x_O$. This reproduces also the experimental observation of Piccolo: [21] the N_2 desorption signal varies slowly with temperature (see Figure 5 of ref 17).

C. CO Beam Transient Signals. The knowledge of the transient signals often allows us to look at the kinetics of the reaction under conditions that cannot be reached in the steady state regime; the concentrations of the adsorbed species can drastically differ from their values at equilibrium. Additional information on the reaction mechanism can thus be obtained in the transient regime.

In Figure 6 is represented the transient signal at 250 °C for an isotropic NO pressure of 10^{-7} Torr. The different curves correspond to various waiting times Δt between the previous CO beam closing at $t = -\Delta t$ and the CO beam opening at $t = 0$. After introducing the CO, one obtains a peak of the CO_2 production rate. The integral of the peak increases with the waiting time. This peak corresponds to the dosage of the initial oxygen at the Pd surface by the CO beam. The integral of this peak is thus directly related to the number of NO molecules dissociated during the time Δt when the CO beam was closed. For long waiting times, the peak integral is constant, indicating that the oxygen coverage under zero CO pressure has reached its maximum value. This value is limited by the slow diffusion of oxygen into the bulk. It is also limited by the reduction of the NO dissociation probability when increasing the coverage. The value for the coverage dependence of the activation energy for NO dissociation used in the simulations has been adjusted with a fit of the corresponding experimental results.[22]

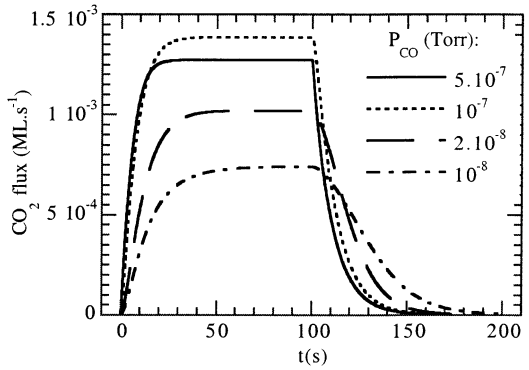

Figure 7. Transient CO_2 production rate at 250 °C. The NO beam flux is equivalent to 5×10^{-8} Torr for different CO pressures. The NO beam is open at $t = 0$ s and closed at $t = 100$ s.

When the initial coverage becomes too high, the sticking coefficient of the CO is not correctly reproduced by our simulations. This mainly affects the shape of the peak but little its integral.

D. NO Beam Transient Signals. Using the same parameters as previously, we have also tried to reproduce the transient regime under NO beam conditions. The time evolution of the CO_2 production rate at $T = 250$ °C is represented in Figure 7, for different isotropic CO pressures. The simulated curves qualitatively agree with the ones obtained on 2.8 nm size particles;[22] no experimental data are available for 10 nm particles. In the high CO pressure regime, the different curves display similar behavior. The higher the CO pressure is, the quicker the steady state conditions are reached. At low CO pressure, the oxygen is not rapidly removed by the CO and its concentration slowly increases with time. This effect has been experimentally evidenced on 2.8 nm particles.[22] The low-pressure curve is very different. In particular, the decay of the CO_2 signal after closing the NO beam is very slow. In the experiment, one observes a slight increase of the CO_2 signal just after closing the NO beam. This is due to the decrease of the NO coverage, which allows further decomposition of the NO molecules and CO_2 production. This qualitative good agreement confirms the hypotheses of the coverage dependence of the activation energy for NO decomposition. At high temperature, the simulated curves display a very similar behavior. In what concerns the decrease of the CO_2 signal after the NO beam is closed, this is in contradiction with the experimental observations on 2.8 nm,[22] which indicates that this part of the signal does not depend on the CO pressure. We never managed to reproduce this behavior, which is certainly related to another type of reaction site, only active at high temperature and especially pronounced on small particles.

V. Conclusion

The comparison between experiments and numerical simulations of the CO + NO reaction on supported Pd particles has evidenced the RLSs of the reaction. At high temperature, the CO_2 production rate is mainly determined by the competition between decomposition and desorption of NO molecules and between oxidation and desorption of CO molecules. At low temperature, the reaction is limited by the decomposition of NO molecules, which is hindered at high coverage. The CO pressure influences in a complex way the CO_2 production rate. This results in particular transient signals.

The theoretical model developed reproduces qualitatively most of the experimental results. It cannot quantitatively describe all of the experimental observations, since approximations have

been made concerning, for example, the coverage dependence of the activation energies or sticking coefficients. In fact, some of the discrepancies observed between the experiments and the simulations result from the fact that the Pd particles have different adsorption sites whereas we have restricted our model to only one type of adsorption site. Even with such approximations, the number of parameters is very high since the reaction is decomposed into six elementary steps. As selective information on specific steps of the reaction have been experimentally obtained, it has been possible to adjust some parameters independently. The agreement with the other experimental results, in particular in what concerns the dependence with temperature and with CO pressure of the steady state TON, is then very good. The model is also validated by the ability of the simulation to describe major features of the transient signals.

References and Notes

(1) Hugo, P. *Ber. Bunsen-Ges. Phys. Chem.* **1970**, *74*, 121.
(2) Fink, Th.; Dath, J.-P.; Imbihl, R.; Ertl, G. *J. Chem. Phys.* **1991**, *95*, 2109.
(3) Zhdanov, V. P.; Kasemo, B. *Surf. Sci. Rep.* **1997**, *29*, 31.
(4) Vesecky, S. M.; Rainer, D. R.; Goodman, D. W. *J. Vac. Sci. Technol. A* **1996**, *14*, 1457.
(5) Daté, M.; Okuyama, H.; Takagi, N.; Nishijima, M.; Aruga, T. *Surf. Sci.* **1996**, *350*, 79.
(6) Kobal, I.; Kimura, K.; Ohno, Y.; Matsushima, T. *Surf. Sci.* **2000**, *445*, 472.
(7) Hirsimäki, M.; Suhonen, S.; Pere, J.; Valden, M.; Pessa, M. *Surf. Sci.* **1998**, *402*−*404*, 187.
(8) Xu, X.; Chen, P.; Goodman, D. W. *J. Phys. Chem.* **1994**, *98*, 9242.
(9) Valden, M.; Aaltonen, J.; Kuusisto, E.; Pessa, M.; Barnes, C. J. *Surf. Sci.* **1994**, *307*−*309*, 193.
(10) Piccolo, L.; Henry, C. R. *Appl. Surf. Sci.* **2000**, *162*−*163*, 670.
(11) Piccolo, L.; Henry; C. R. *J. Mol. Catal. A* **2001**, *167*, 181.
(12) Rainer, D. R.; Vesecky, S. M.; Coranne, M.; Oh, W. S.; Goodman, D. W. *J. Catal.* **1997**, *167*, 234.
(13) Hammer, B. *J. Catal.* **2001**, *199*, 171.
(14) Henry, C. R.; Chapon, C.; Goyhenex, C.; Monot, R. *Surf. Sci.* **1992**, *272*, 283.
(15) Duriez, C.; Henry, C. R.; Chapon, C. *Surf. Sci.* **1991**, *253*, 190.
(16) Henry, C. R.; Chapon, C.; Duriez, C. *J. Chem. Phys.* **1991**, *95*, 700.
(17) Piccolo, L.; Henry, C. R. *Surf. Sci.* **2000**, *452*, 198.
(18) Becker, C.; Henry, C. R. *Surf. Sci.* **1996**, *352*−*354*, 457.
(19) Becker, C.; Henry, C. R. *Catal. Lett.* **1997**, *43*, 55.
(20) Piccolo, L.; Becker, C.; Henry, C. R. *Appl. Surf. Sci.* **2000**, *164*, 156.
(21) Piccolo, L. Ph.D. Thesis, University of Aix-Marseille II, 1999.
(22) Prévot, G.; Meerson, O.; Piccolo, L.; Henry, C. R. *J. Phys.: Condens. Matter* **2002**, *14*, 4251.
(23) Permana, H.; Ng, K. Y. S.; Peden, C. H. F.; Schmieg, S. J.; Lambert, D. K.; Belton, D. N. *J. Catal.* **1996**, *164*, 194.
(24) Sharpe, R. G.; Bowker, M. *Surf. Sci.* **1996**, *360*, 21.
(25) Xu, X.; Goodman, D. W. *Catal. Lett.* **1994**, *24*, 31.
(26) Meusel, I.; Hoffmann, J.; Hartmann, J.; Heemei, M.; Bäumer, M.; Libuda, J.; Freund, H. J. *Catal. Lett.* **2001**, *71*, 5.
(27) Bondzie, V. A.; Kleban, P.; Dwyer, D. J. *Surf. Sci.* **1996**, *347*, 319.
(28) Leisenberger, F. P.; Koller, G.; Sock, M.; Surnev, S.; Ramsey, M. G.; Netzer, F. P.; Klötzer, B.; Hayek, K. *Surf. Sci.* **2000**, *445*, 380.
(29) Henry, C. R. *Surf. Sci. Rep.* **1998**, *31*, 231.
(30) Zhdanov, V. P.; Kasemo, B. *Surf. Sci. Rep.* **2000**, *39*, 25.
(31) Hammer, B.; Nørskov, J. K. *Adv. Catal.* **2000**, *45*, 71.
(32) Matolin, V.; Stara, I. *Surf. Sci.* **1998**, *398*, 117.
(33) Eriksson, M.; Ekedahl, L.-G. *Surf. Sci.* **1998**, *412*−*413*, 430.
(34) Conrad, H.; Ertl, G.; Küppers, J. *Surf. Sci.* **1978**, *76*, 323.
(35) Engel, T. *J. Chem. Phys.* **1978**, *69*, 373.
(36) Schmick, H.-D.; Wassmuth, H.-W. *Surf. Sci.* **1982**, *123*, 471.
(37) Yeo, Y. Y.; Vattuone, L.; King, D. A. *J. Chem. Phys.* **1997**, *106*, 1990.